ISSN 0567-7718, Volume 26, Number 1

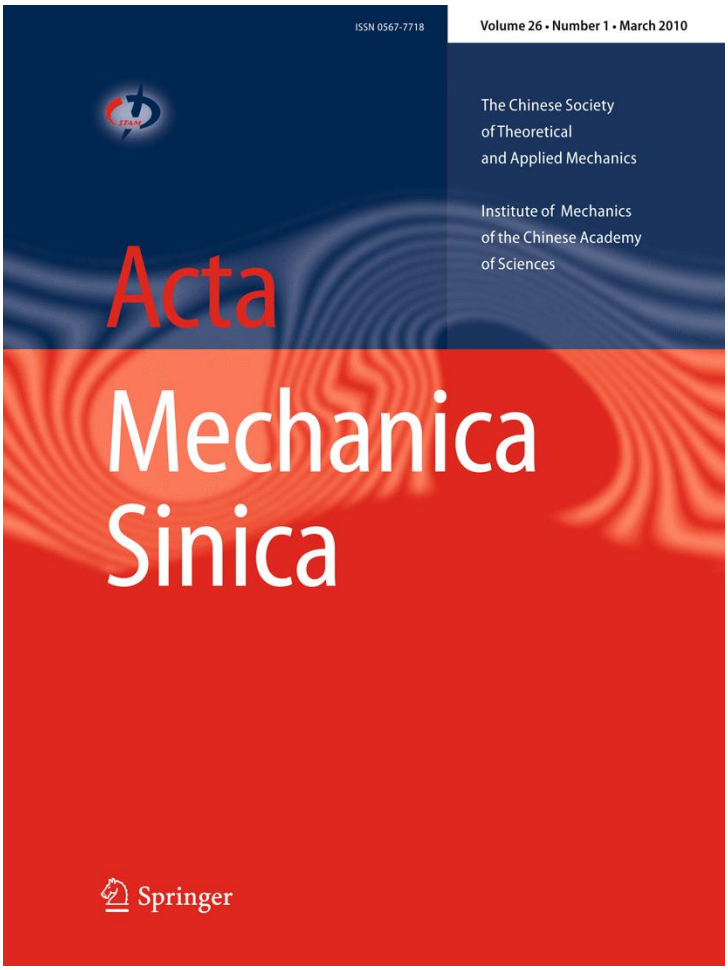

Acta Mech Sin (2010) 26:27–35
DOI 10.1007/s10409-009-0310-2

RESEARCH PAPER

Characterization of cuttlebone for a biomimetic design of cellular structures

Joseph Cadman · Shiwei Zhou · Yuhang Chen · Wei Li · Richard Appleyard · Qing Li

Received: 16 June 2009 / Accepted: 3 August 2009 / Published online: 12 November 2009

Abstract Cuttlebone is a natural material possessing the multifunctional properties of high porosity, high flexural stiffness and compressive strength, making it a fine example of design optimization of cellular structures created by nature. Examination of cuttlebone using scanning electron microscopy (SEM) reveals an approximately periodic microstructure, appropriate for computational characterization using direct homogenization techniques. In this paper, volume fractions and stiffness tensors were determined based on two different unit cell models that were extracted from two different cuttlefish samples. These characterized results were then used as the target values in an inverse homogenization procedure aiming to re-generate microstructures with the same properties as cuttlebone. Unit cells with similar topologies to the original cuttlebone unit cells were achieved, attaining the same volume fraction (i.e. bulk density) and the same (or very close) stiffness tensor. In addition, a range of alternate unit cell topologies were achieved also attaining the target properties, revealing the non-unique nature of this inverse homogenization problem.

Keywords Inverse homogenization · Cuttlebone microstructure · Topology optimization · Scanning electronic microscopy (SEM) · Extra-light biomaterials

J. Cadman · S. Zhou · Y. Chen · W. Li · Q. Li (✉)
School of Aerospace, Mechanical and Mechatronic Engineering, The University of Sydney, Sydney, NSW 2006, Australia
e-mail: Q.Li@usyd.edu.au

R. Appleyard
Faculty of Medicine, The University of Sydney, Sydney, NSW 2006, Australia

1 Introduction

Many marine species exhibit extraordinary mechanical and physical properties. For example, the microstructure of cuttlebone possesses the multifunctional properties of high porosity, high flexural stiffness and compressive strength, which provides us with a fine example of design optimization of cellular structures created by nature. Cuttlebone requires sufficient porosity to maintain neutral buoyancy at habitation depths, at the same time maintaining enough stiffness and strength to prevent severe distortion under fluidic force under water and crushing under high hydrostatic pressure [1].

Previous approaches in determining the properties of cuttlebone typically include: microscopic observation, mechanical testing, chemical analysis, and predictive models based on pillar buckling or plate strength [1–4]. In such traditional contexts of characterization, Birchall and Thomas [2] developed a thorough physical and chemical description of cuttlebone and also conducted tests to determine the mechanical properties of the cuttlebone. Gower and Vincent [4] sought to characterize the physical and mechanical properties of cuttlebone by considering morphological differences between several different species of cuttlefish known to inhabit different ocean depths. A mathematical model based on pillar buckling was developed in an attempt to predict the impact of these morphological differences on habitation depths for various species of cuttlefish. A similar attempt to predict the maximum habitation depth for various species of cuttlefish was made by Sherrard [1], who developed an alternative mathematical model based on a simple plate theory model. These predictive models reveal a small factor-of-safety for cuttlebone due to implosion indicative of the stability of the aquatic environment [1,4]. However, this could also be attributed to the non-catastrophic, layer by layer failure of the cuttlebone under compression [2,4].

More recently, cuttlebone has been used in developing superconducting materials [5] and tissue engineering scaffolds [6–9], earmarking it as an extraordinary microstructural material with great potential in many new applications. Cuttlebone was deemed appropriate for use as a superconductor template due to its high porosity, making fabrication processes easier. Yttrium barium superconductors were created possessing critical current densities two orders of magnitude higher than equivalent commercially available products. Although the cuttlebone microstructure was preserved in the process, the resultant strength was an issue. In order to achieve reasonable strength, silver doping was required, which leads to a negative impact on the critical current density [5].

Cuttlebone has also been converted directly into hydroxyapatite (HA) tissue scaffolds via hydrothermal transformation [6,8,9]. These scaffolds well maintained the cuttlebone microstructure and exhibit ideal pore size ($\sim 100-200\mu$m) and interconnectivity to support biological activities in tissue regeneration, which has been verified by in vitro testing [8]. The scaffolds can also be easily machined at any stage of the transformation process [8].

Whilst the above studies demonstrate the vast potential of cuttlebone as a new class of engineering material or template, some questions remain open. Strength appears to be an issue in both the studies on superconductors and scaffolds. Would it therefore be beneficial to reproduce such special microstructures, adopting different base materials to see if better bulk mechanical properties can be attained? Also, what happens if the required macroscopic dimensions exceed those that can be machined from natural cuttlebone? If this special microstructure can be reproduced by replicating unit cells extracted from the cuttlebone samples, there will be less physical limitations on macroscopic dimensions, thereby widening its spectrum of applications.

These areas of research could benefit from a thorough understanding of the relationship between the mechanical properties and microstructure of cuttlebone. Given a primary periodicity of the cuttlebone cellular structure, the stiffness tensor of the cuttlebone unit cell (or smallest representative volume element, RVE) can, on the one hand, be approximately determined via the direct homogenization technique. On the other hand, the characterized stiffness tensor can be then re-attained using a so-called inverse homogenization method in the same unit cell. As such, material designs that share the mechanical properties of cuttlebone can be easily fabricated using state-of-the-art Solid Free-Form Fabrication (SFF) techniques [10]. The present paper aims to provide a demonstrative solution to such a biomimetic design problem by re-creating the superior microstructural properties of cuttlebone in a computational framework. Although the final goal of this research is to test the viability of incorporating such cellular structures into scaffold tissue engineering applications as attempted experimentally in Refs. [6–9], such biomimetic cellular structures could have potential in more novel applications.

2 Materials and methods

2.1 Cuttlebone sample and SEM images

Cuttlebone samples were obtained from Sydney beaches, Australia. These samples were all in a fairly good condition with minimal external damage. Species is unidentified and a comparable study is beyond the scope of this study.

The samples were prepared in two different ways. Some samples were simply snapped along the relevant planes (it was found that the material is very brittle). Alternative samples were cut along the various planes using a scalpel. All the samples were sputter coated with 20 nm of gold.

Images of cuttlebone were captured using scanning electronic microscopy (SEM) (Philips 505 SEM, Everhart-Thornley detector, 20 kV acceleration voltage). Transverse section (A–A) images were obtained from three separate cuttlebone samples as shown in Fig. 1.

2.2 Extraction of unit cell for modeling

The transverse section (refer to Fig. 1) of the cuttlebone reveals an approximately periodic microstructural pattern, as seen in the snapshot in Fig. 2, making the material a good candidate for computational characterization via the direct homogenization. Different unit cells with different sizes and aspect ratios were extracted directly from the SEM images acquired.

The original image was cropped so that only the unit cell of interest remained. This was converted into the binary data, which could then be manipulated using image processing functions to better reflect the original sectional topology of the cuttlebone unit cell. The resulting image displays nearly vertical symmetry. In order to simplify the analysis, the vertical symmetry was imposed by reflecting the left half of the image (Fig. 2). The result of this process was a 0–1 matrix

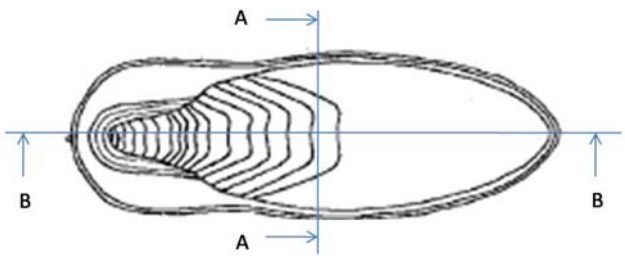

Fig. 1 Cuttlebone in planar view showing transverse section (A–A) and longitudinal section (B–B)

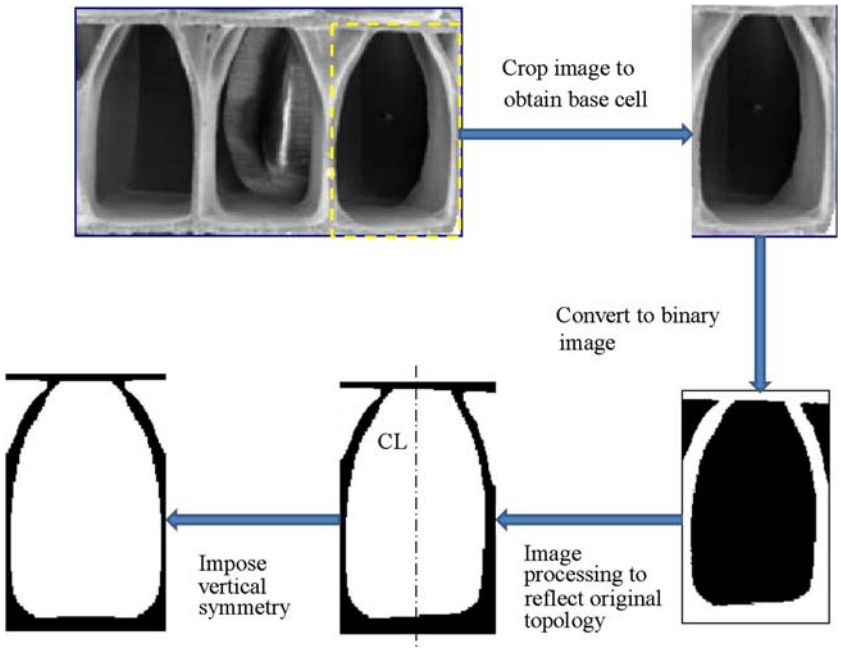

Fig. 2 Schematic showing the steps in obtaining a solid-void image reflecting unit cell topology (CL is an abbreviation for centerline)

describing the void-solid representation of the cuttlebone unit cell, which will be used directly for computing the mechanical properties via the homogenization technique.

2.3 Problem formulation

In this paper, the material characterization and design involve two distinct problems: direct homogenization that aims to determine the mechanical properties of cuttlebone; and inverse homogenization that aims to design microstructures with the same mechanical properties as cuttlebone.

The former allows directly calculating the effective properties from the given composition and configuration of the smallest representative unit (or unit cell) by applying a double-scale asymptotic expansion and the assumption of periodicity [11]. For simplified microstructures, the effective properties can be derived analytically [12]. However, for more complicated microstructures, like those considered in this study, the homogenization method must be employed within the framework of finite element analysis [13].

The latter seeks a proper microstructural architecture of a unit cell satisfying a set of specified physical properties within a topology optimization framework. Sigmund [14] was the first to extend topology optimization with homogenization into the realm of microstructural material design; a technique commonly termed "inverse homogenization". Since its inception, the inverse homogenization has developed into a powerful tool capable of producing a full array of microstructural materials with various targeted and extreme properties.

2.3.1 Direct homogenization

The homogenization technique calculates the physical properties, e.g. effective stiffness tensor, C^{H}_{ijkl}, from the given structure and composition of a unit cell as [11,13]

$$C^{\mathrm{H}}_{ijkl}(\rho) = \frac{1}{|\Omega|}\int_{\Omega} C_{ijmn}(\rho)(\varepsilon^{0(kl)}_{mn} - \varepsilon^{*(kl)}_{mn})\mathrm{d}\Omega, \tag{1}$$

where $|\Omega|$ denotes the area of the design domain Ω (unit cell); C_{ijmn} denotes the stiffness tensor of the base material, which is assumed to be isotropic. For brevity, the volume fraction of solid phase $\rho(\boldsymbol{x})$ (also named the relative density) within a local finite element centered at point $\boldsymbol{x} \in \Omega$ is denoted by ρ. Obviously, the solid and void elements can be expressed in $\rho = 1$ and $\rho = 0$, respectively.

In order to obtain the characteristic strain fields $\varepsilon^{*(kl)}_{mn}$, four linearly independent unit test strain fields $\varepsilon^{0(11)}_{mn} = (1\ \ 0\ \ 0\ \ 0)^{\mathrm{T}}$, $\varepsilon^{0(22)}_{mn} = (0\ \ 1\ \ 0\ \ 0)^{\mathrm{T}}$, $\varepsilon^{0(12)}_{mn} = (0\ \ 0\ \ 1\ \ 0)^{\mathrm{T}}$ and $\varepsilon^{0(21)}_{mn} = (0\ \ 0\ \ 0\ \ 1)^{\mathrm{T}}$ are applied to the unit cell. The solution to the following characteristic equation

$$\int_{\Omega} C_{ijmn}\varepsilon_{ij}(v)\varepsilon^{*(kl)}_{mn}\mathrm{d}\Omega = \int_{\Omega} C_{ijmn}\varepsilon_{ij}(v)\varepsilon^{0(kl)}_{mn}\mathrm{d}\Omega, \tag{2}$$

determines $\varepsilon^{*(kl)}_{mn}$, where the virtual displacement field $v \in H_{\mathrm{per}}$ belongs to the periodic Sobolev functional space [15,16].

The base material of the cuttlefish bone is assumed to be isotropic with only two elastic parameters, namely the Poisson's ratio υ_0 and Young's modulus E_0. Unlike the Poisson's ratio, which is independent of the relative density,

the local Young's modulus is a variable related to the volume fraction of solid phase ρ. As the relative density needs to be relaxed to an intermediate value in the design process (i.e. $0 < \rho < 1$, denoting the existence of some elements mixed with solid and void phases), appropriate interpolation of the local Young's modulus becomes crucial. A good interpolation scheme should firstly guarantee the convergence of the relative density to 0 or 1 in the final step, and secondly abide by the Hashin-Shtrikman (HS) theoretical bounds of material [17–19]. One of the most often used models is the solid isotropic microstructure with penalty (SIMP), in which $E(\rho) = \rho^p E_0$ [17]. To meet the upper HS bound, the penalty factor should be $p \geq 3$ [17]. In the present paper, the results were generated using both the SIMP and the upper HS bound interpolation schemes, which takes the form of

$$E(\rho) = E_{\text{void}} + \frac{2\rho\, E_{\text{void}}(E_0 - E_{\text{void}})}{2E_{\text{void}} + (1-\rho)(E_0 - E_{\text{void}})}, \tag{3}$$

where E_{void} is the Young's modulus of the void material, which should be a very low value other than zero (e.g. $E_{\text{void}} = 0.001$) to computationally avoid singularity in finite element analysis.

In the present study a Poisson's ratio of 0.25 was used for the base solid material. This value was used by Gower and Vincent [4]. A Young's modulus of 1 unit was assigned to the base material in order to obtain dimensionless results.

2.3.2 *Inverse homogenization*

An inverse homogenization is typically formulated as the least squares of the difference between the entries of the target stiffness tensor C^*_{ijkl} and the homogenized stiffness tensor C^{H}_{ijkl}. In this paper, the effective stiffness tensor of the cuttlebone unit cell, characterized via the direct homogenization, is adopted as the target stiffness tensor, and an additional constraint on the volume fraction is added to the problem, which is formulated as

$$\begin{aligned} &\min_{\rho} J(\rho) = \sum_{i,j,k,l=1}^{3} r_{ijkl}(C^*_{ijkl} - C^{\text{H}}_{ijkl})^2, \\ &\text{subject to} \quad \int_{\Omega} \rho \mathrm{d}\Omega = V_0, \end{aligned} \tag{4}$$

where r_{ijkl} are positive weighting factors used to emphasize the role of different entries in the objective function, and V_0 is the volume fraction constraint of the real cuttlebone unit cell.

To use the method of moving asymptotes (MMA) [20] for solving the optimization problem, Eq. 4, the sensitivity of the objective function is evaluated as

$$\frac{\partial J}{\partial \rho} = -2 \sum_{i,j,k,l=1}^{3} r_{ijkl}(C^*_{ijkl} - C^{\text{H}}_{ijkl}) \frac{\partial C^{\text{H}}_{ijkl}}{\partial \rho}, \tag{5}$$

where $\partial C^{\text{H}}_{ijkl}/\partial\rho$ can be derived according to the adjoint variable method [21] as

$$\partial C^{\text{H}}_{ijkl}/\partial\rho = (1 - \varepsilon^{*(ij)}_{mn}) \frac{\partial}{\partial \rho} C_{ijmn} (1 - \varepsilon^{*(kl)}_{mn}). \tag{6}$$

A common problem in finite element based topology optimization is the appearance of checkerboard patterns and mesh dependency. Numerous methods are available to eliminate such numerical instability problems. Filtering techniques [22] and perimeter constraints [23,24] are some typical methods. However, filtering techniques do not normally allow for a sharp boundary representation while the perimeter constraints can be difficult to implement, relying on trial and error to determine appropriate constraint values. The non-linear diffusion technique [25] has been proven fairly

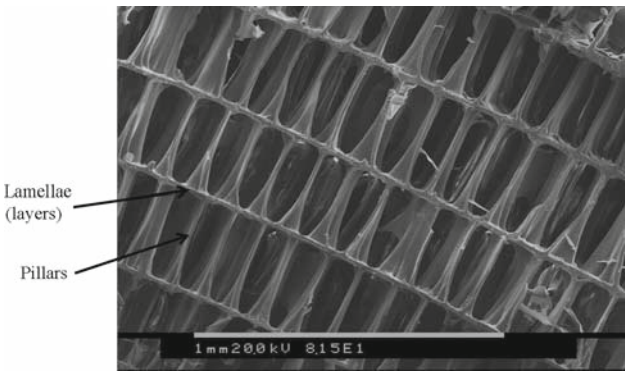

Fig. 3 Transverse section of cuttlebone sample at 81.5× magnification identifying lamellae and pillars (*length scale* of 1 mm is associated with the white portion of the *horizontal bar*)

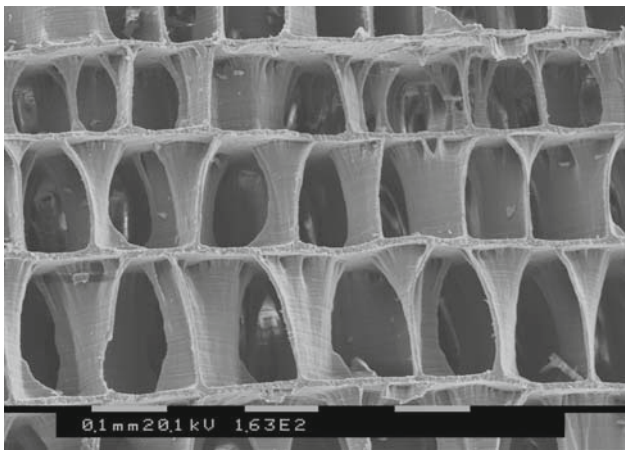

Fig. 4 Transverse section of cuttlebone sample at 163× magnification showing varying aspect ratios (*length scale* of 0.1 mm is associated with the white portions of the *horizontal bar*)

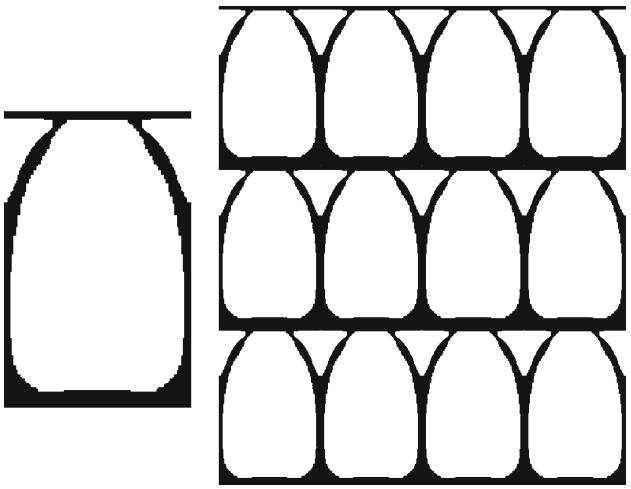

Fig. 5 Target unit cell model extracted from SEM image and corresponding periodic representation for Ex. 1

effective for removing mesh dependency, checkerboard patterns and maintaining a sharp material boundary [15,18,19,26–29] and is, therefore, adopted in this study.

The non-linear diffusion technique introduces an extra term to the objective function as

$$\min_{\rho} J(\rho) = \sum_{i,j,k,l=1}^{3} r_{ijkl}(C^{*}_{ijkl} - C^{\mathrm{H}}_{ijkl})^2 + \varepsilon^2 \varphi(\|\nabla\rho\|), \tag{7}$$

where ε is a small positive weighting factor controlling the effect of the non-liner diffusion and $\varphi(\|\nabla\rho\|)$ is the diffusion energy dependent on the norm of the density gradient $\|\nabla\rho\|$.

3 Results and discussion

3.1 Microscopic observation

The images captured using SEM exhibit the significant morphological features previously identified in Refs.[1,2,4], where the lamellae (or layers) of the base material are separated and connected by pillars (Fig. 3).

Table 1 Characterization of target stiffness tensor and volume fraction for given aspect ratio and comparison with results from inverse homogenization design in Ex. 1 (*nx* and *ny* denote the number of elements in *x* and *y* directions, V_0 the constraint of volume fraction in percentage and C_{ijkm} the components of the stiffness tensor in dimensionless units)

	ny	*nx*	$V_0/\%$	C_{1111}	C_{1122}	C_{1133}	C_{2222}	C_{2233}	C_{1212}
Target	130	206	20.45	0.0864	0.0131	0.0000	0.0965	0.0000	0.0018
Design	64	103	20.45	0.0767	0.0159	0.0000	0.0881	0.0000	0.0020

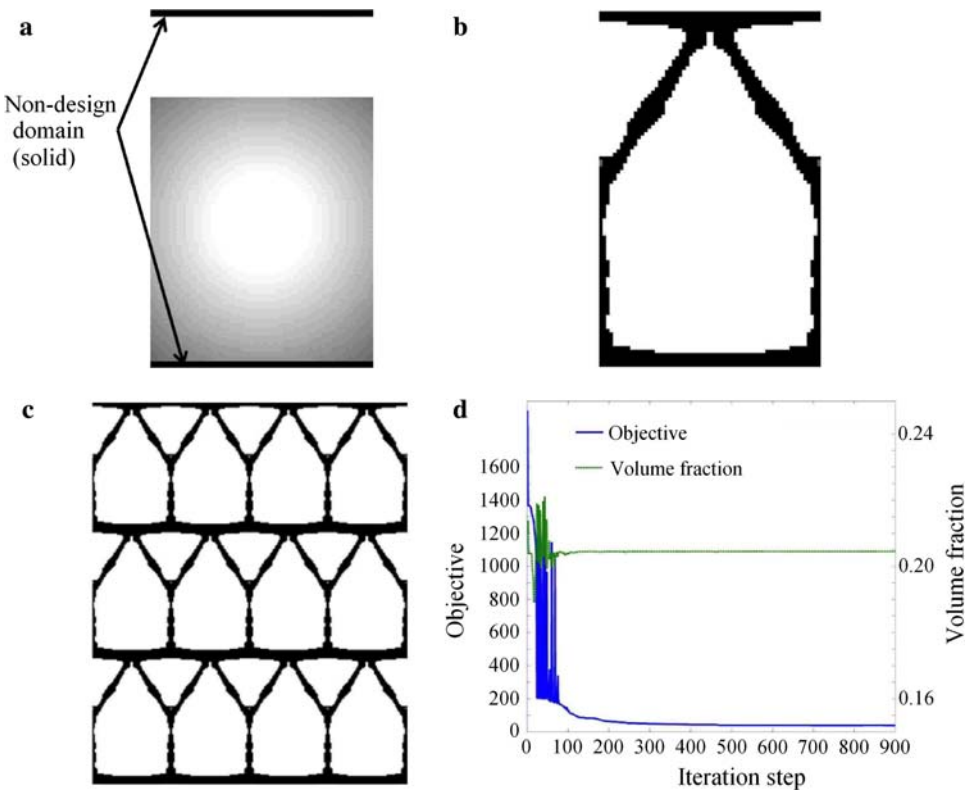

Fig. 6 **a** Initial guess; **b** Final unit cell design; **c** Periodic representation; **d** Convergence history for Ex. 1

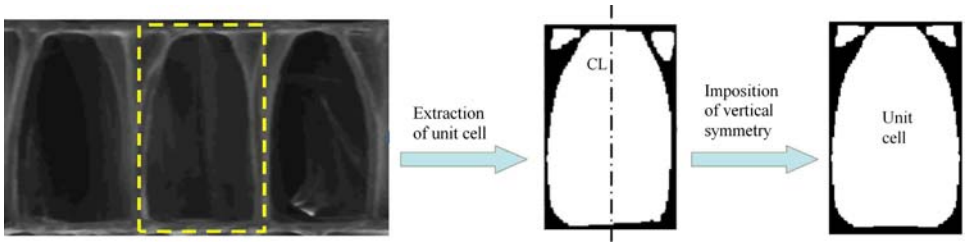

Fig. 7 Schematic showing steps in obtaining a solid-void image of unit cell topology in Ex. 2 (note that CL is the abbreviation for centerline)

Table 2 Characterization of target stiffness tensor and volume fraction for given aspect ratio and comparison with results from inverse homogenization design in Ex. 2 (*nx* and *ny* denote the number of elements in *x* and *y* directions, V_0 the constraint of volume fraction in percentage and C_{ijkm} the components of the stiffness tensor in dimensionless units)

	ny	*nx*	$V_0/\%$	C_{1111}	C_{1122}	C_{1133}	C_{2222}	C_{2233}	C_{1212}
Target	126	202	21.69	0.0907	0.0061	0.0000	0.0779	0.0000	0.0015
Design	60	100	21.69	0.0907	0.0061	0.0000	0.0779	0.0000	0.0015

There are a number of additional geometrical features that are identifiable in the SEM images. Inspection of the transverse section (Fig. 3) reveals an approximately periodic microstructure, making this material a good candidate for direct characterization via the homogenization technique. Also, Fig. 4 shows that in some of our samples the aspect ratio of the unit cells change from layer to layer. Therefore, the effective properties should be characterized for different aspect ratios of unit cells. In this paper, only two different aspect ratios are considered. The further study of such graded effective properties is beyond the scope of this paper and the reader can consult [29].

3.2 Demonstrative examples

The design domains in all examples are discretized into square elements with *ny* and *nx* divisions along the horizontal and vertical directions, respectively. In 2D, only six independent entries (see Tables 1, 2) of the stiffness tensor are considered. The second and third rows in these tables give the target and attained values, respectively. Due to the limitation of the available computer resource, all examples were conducted using a relatively coarse mesh when compared to the raw pixel data extracted from the SEM images.

3.2.1 Example 1

In the first example, the unit cell was extracted from the SEM image shown in Fig. 2. The dimensionless effective stiffness tensor was calculated via the direct homogenization. The volume fraction is defined in sect. 2.3 and is also dimensionless. The results are summarized in Table 1.

For the inverse homogenization, a range of initial designs were tested with or without prescription of non-design domains to observe the effect on the final topologies. The final topological design which most resembles the target unit cell topology (Fig. 5) is shown in Fig. 6.

Table 1 shows that, for the designed microstructure, the volume fraction converged well and the components of the stiffness tensor closely attained the target values that were characterized from the SEM-homogenization procedure presented. From a geometric perspective, there are some degrees of difference in the top arch shape between the resultant topology (Fig. 6) and the target unit cell topology (Fig. 5). However, the major topological features are well retained. When the designed unit cell is assembled in a periodic fashion, the overall topology bears a closer resemblance.

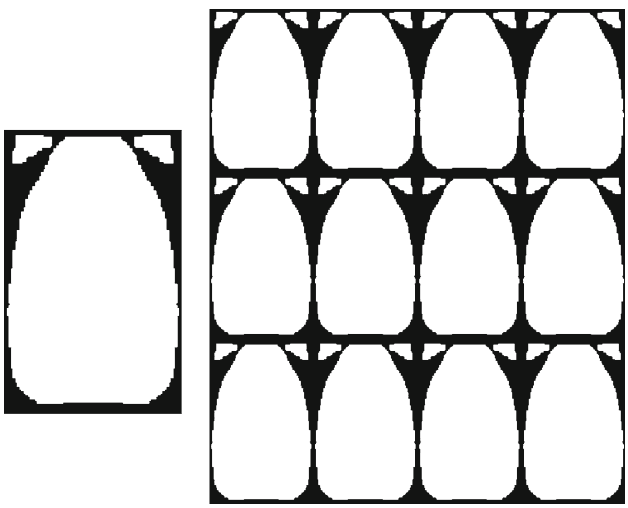

Fig. 8 Target unit cell model extracted from SEM image and corresponding periodic representation for Ex. 2

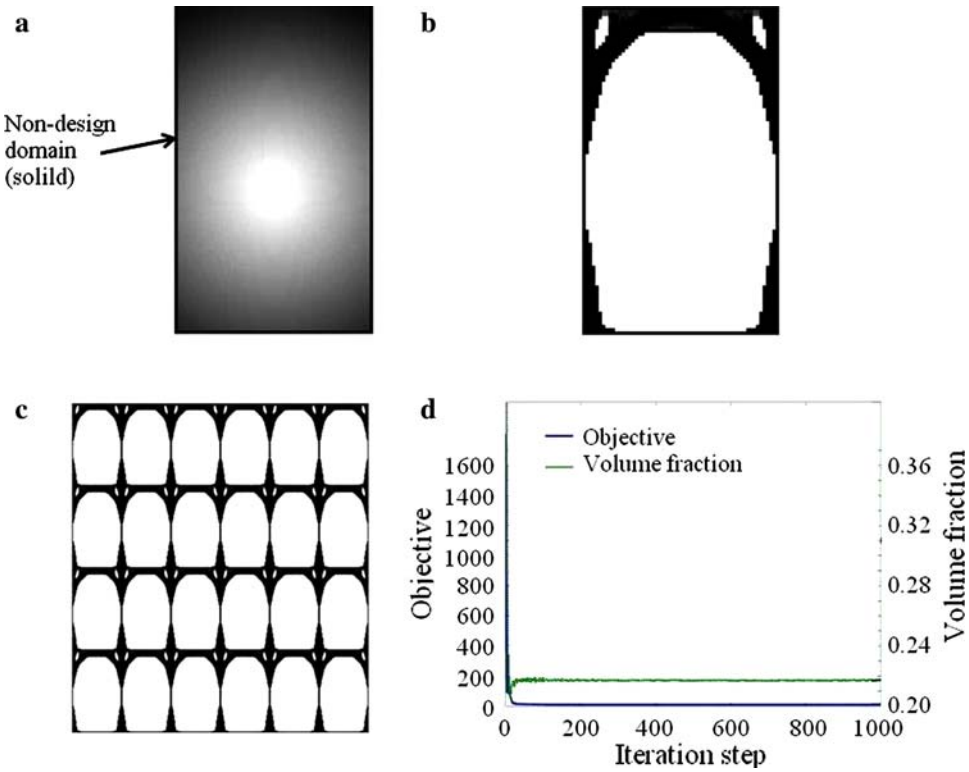

Fig. 9 **a** Starting guess; **b** Final unit cell design; **c** Periodic representation; **d** Convergence history for Ex. 2

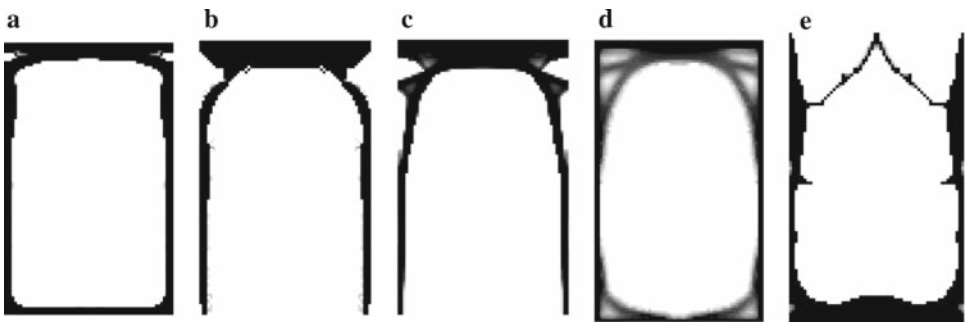

Fig. 10 Alternate topologies for Ex. 1 (**a**, **b** and **c**) and Ex. 2 (**d** and **e**) that have very close stiffness tensors to the target values

3.2.2 Example 2

In the second example, the unit cell was extracted from a different SEM image as shown in Fig. 7 with vertical symmetry imposed. The dimensionless effective stiffness tensor was calculated via the direct homogenization. The volume fraction is defined in sect. 2.3 and is also dimensionless. The results are listed in Table 2.

Again, a range of initial designs were tested for the inverse homogenization with or without prescribed non-design domains to observe the effect on the final topologies. The final design with the topology most resembling the target unit cell topology (Fig. 8) is shown in Fig. 9.

Table 2 shows that, for the designed microstructure, the volume fraction and all elasticity components attained the target values quite well. From a topological perspective, the main difference between the resultant configuration (Fig. 9) and the target unit cell architecture acquired from SEM (Fig. 8) is the formation of the holes in the top corners. However, the significant geometric features are retained in the final design. When arranging the designed unit cell in a periodic fashion, again, the overall topology bears a closer resemblance.

3.2.3 Non-uniqueness of solutions

By using a variety of different initial designs with/without the use of non-design domains, a range of different final topologies were produced using the inverse homogenization. This highlights to the non-uniqueness of the solution

to this optimization problem. Shown in Fig. 10 are a range of alternative unit cell topologies that are yielded from the inverse homogenization. All these topologies attained the target volume fraction and stiffness tensor very closely, but were excluded from the above discussion due to more significant differences in geometry. Nevertheless, there does exist certain similarity in their configuration, where the solid material is mainly distributed around the sides of the unit cells except some top corners. It is noted that although Figs. 10b, c and e appear very different from others in Exs. 1 and 2, respectively, they could still exhibit topological similarity if assembling them periodically. This implies that the significant difference in unit cell may not necessarily mean remarkable difference in materialized structures.

4 Concluding remarks

This paper develops the capability of analyzing the properties of cuttlebone using the direct homogenization technique, by realizing that the transverse section has an approximately periodic microstructure. This paper also shows the feasibility of using the inverse homogenization techniques to re-generate microstructural architectures sharing the same volume fraction (density) and stiffness tensor as the cuttlebones for various target designs. While the attained geometries are not identical, strong topological similarities can be observed in the corresponding unit cells and assembled microstructures.

Using the same analysis to investigate the effective properties and resultant microstructures for different aspect ratios has been left for subsequent research in developing functionally graded materials (FGM) [29]. Also development of a 3D model using proper respective images to mimic other physical properties of cuttlebone will be considered in the future.

This study has shown that it is possible to develop biomimetic microstructural materials which share the same properties as nature materials like cuttlefish backbone. It is anticipated that such biomimetic materials will have a significant impact in a number of technological fields like scaffold tissue engineering, superconductors and extra lightweight cellular structures.

Acknowledgements This study was supported by Australian Research Council Discovery Project grant. The first author is grateful for the University Postgraduate Award (UPA) at The University of Sydney.

References

1. Sherrard, K.M.: Cuttlebone morphology limits habitat depth in eleven species of Sepia (Cephalopoda: Sepiidae). Biol. Bull. **198**, 404–414 (2000)
2. Birchall, J.D., Thomas, N.L.: On the architecture and function of cuttlefish bone. J. Mater. Sci. **18**, 2081–2086 (1983)
3. Re, P., Narciso, L.: Growth and cuttlebone microstructure of juvenile cuttlefish, sepia-officinalis, under controlled conditions. J. Exp. Mar. Biol. Ecol. **177**, 73–78 (1994)
4. Gower, D., Vincent, J.F.V.: The mechanical design of the cuttlebone and its bathymetric implications. Biomimetics **4**, 37–57 (1996)
5. Culverwell, E., Wimbush, S.C., Hall, S.R.: Biotemplated synthesis of an ordered macroporous superconductor with high critical current density using a cuttlebone template. Chem. Commun. **9**, 1055–1057 (2008)
6. Rocha, J.H.G. et al.: Hydrothermal growth of hydroxyapatite scaffolds from aragonitic cuttlefish bones. J. Biomed. Mater. Res. A **77**, 160–168 (2006)
7. Kannan, S. et al.: Fluorine-substituted hydroxyapatite scaffolds hydrothermally grown from aragonitic cuttlefish bones. Acta Biomater. **3**, 243–249 (2007)
8. Rocha, J.H.G. et al.: Scaffolds for bone restoration from cuttlefish. Bone **37**, 850–857 (2005)
9. Rocha, J.H.G. et al.: Hydroxyapatite scaffolds hydrothermally grown from aragonitic cuttlefish bones. J. Mater. Chem. **15**, 5007–5011 (2005)
10. Hutmacher, D.W., Sittinger, M., Risbud, M.V.: Scaffold-based tissue engineering: rationale for computer-aided design and solid free-form fabrication systems. Trends Biotechnol. **22**, 354–362 (2004)
11. Hassani, B., Hinton, E.: A review of homogenization and topology optimization I—homogenization theory for media with periodic structure. Comput. Struct. **69**, 707–717 (1998)
12. Feng, X.Q., Mai, Y.W., Qin, Q.H.: A micromechanical model for interpenetrating multiphase composites. Comput. Mater. Sci. **28**, 486–493 (2003)
13. Bendsoe, M.P., Kikuchi, N.: Generating optimal topologies in structural design using a homogenization method. Comput. Methods Appl. Mech. Eng. **71**, 197–224 (1988)
14. Sigmund, O.: Materials with prescribed constitutive parameters—an inverse homogenization problem. Int. J. Solids Struct. **31**, 2313–2329 (1994)
15. Zhou, S.W., Li, Q.: Design of graded two-phase microstructures for tailored elasticity gradients. J. Mater. Sci. **43**, 5157–5167 (2008)
16. de Kruijf, N. et al.: Topological design of structures and composite materials with multiobjectives. Int. J. Solids Struct. **44**, 7092–7109 (2007)
17. Bendsoe, M.P., Sigmund, O.: Material interpolation schemes in topology optimization. Arch. Appl. Mech. **69**, 635–654 (1999)
18. Zhou, S.W., Li, Q.: Computational design of microstructural composites with tailored thermal conductivity. Numer. Heat Transf. A **54**, 686–708 (2008)
19. Zhou, S.W., Li, Q.: A microstructure diagram for known bounds in conductivity. J. Mater. Res. **23**, 798–811 (2008)
20. Svanberg, K.: The method of moving asymptotes—a new method for structural optimization. Int. J. Numer. Methods Eng. **24**, 359–373 (1987)
21. Haug, E.J., Choi, K.K., Komkov, V.: Design Sensitivity Analysis of Structural Systems. United States: Academic Press, Orlando (1986)
22. Sigmund, O.: On the design of compliant mechanisms using topology optimization. Mech. Struct. Mach. **25**, 493–524 (1997)
23. Haber, R.B., Jog, C.S., Bendsoe, M.P.: A new approach to variable-topology shape design using a constraint on perimeter. Struct. Optim. **11**, 1–12 (1996)
24. Fernandes, P., Guedes, J.M., Rodrigues, H.: Topology optimization of three-dimensional linear elastic structures with a constraint on "perimeter". Comput. Struct. **73**, 583–594 (2006)
25. Aubert, G., Kornprobst, P.: Mathematical Problems in Image Processing: Partial Differential Equations and the Calculus of Variations. Appl. Math. Sci. Springer, New York (2006)

26. Zhou, S.W., Li, Q.: The relation of constant mean curvature surfaces to multiphase composites with extremal thermal conductivity. J. Phys. D Appl. Phys. **40**, 6083–6093 (2007)
27. Zhou, S.W., Li, Q.: Computational design of multi-phase microstructural materials for extremal conductivity. Comput. Mater. Sci. **43**, 549–564 (2008)
28. Zhou, S.W., Li, Q.: Design of graded two-phase microstructures for tailored elasticity gradients. J. Mater. Sci. **43**, 5157–5167 (2008)
29. Zhou, S.W., Li, Q.: Microstructural design of connective base cells for functionally graded materials. Mater. Lett. **62**, 4022–4024 (2008)